AMSI VACATION RESEARCH SCHOLARSHIPS 2022–23

SET YOUR SIGHTS ON RESEARCH THIS SUMMER

Mathematical modelling and simulation of stress fibers in living cells

Timothy Ryall

Supervised by Dietmar Oelz

University of Queensland

AMSI AUSTRALIAN MATHEMATICAL SCIENCES INSTITUTE

Contents

Abstract

In a recent honours thesis an 1D model of a stress fibre was developed and an associated agent based model was derived for the purpose of simulating the fibres and its components. This model accounted for the interactions of actin filaments and associated proteins (molecular motors, cross-linker) and proposed "early motor drop-offs" as an explanation to the contraction of fibres seen in nature. We aim to determine and derive the effect of early motor drop-offs on the contraction of stress fibres. We preform a computational study of the contractile force generated by the stress fibre relative to motor drop off distance. We also derive an appropriate homogenisation limit of the agent based model and compute a closed form expression for the effective contractile force

Introduction

Stress fibres are contractile structures that are found in many non-muscle cells consisting of dense bundles of microscopic filaments [7]. They enable cell movement through the expansion and contraction of the fibres via the interactions between the filaments that make up the bundle . However, within stress fibres these structures are highly packed and cannot be tracked using microscopy. Therefore we use modelling and simulation to gain insight.

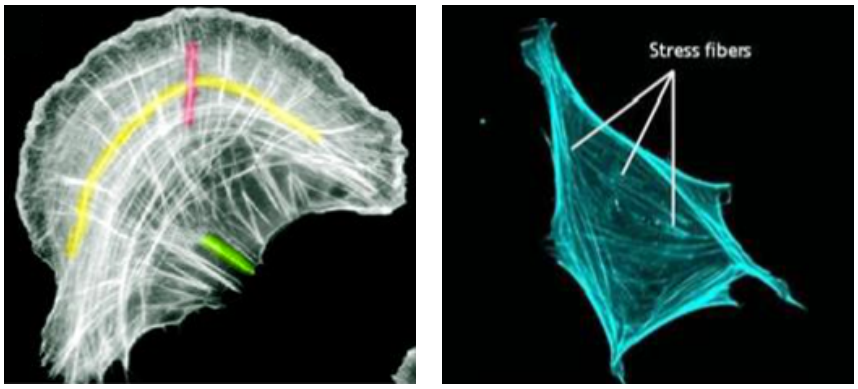

(a) Wei Wei Luo, Mechanobiology Institute, Singapore

(b) Sari Tojkander, institute of Biotechnology, Finland

Figure 1: Examples of stress fibres in cells

Both in vivo and in vitro assays ahve shown that three molecular players - actin filaments, myosin-II motors pulling actin filaments together, and actin cross-linking proteins - are essential for contraction and make up our dense stress fibre bundle however it is difficult to visualise how stress fibres preform this contraction and hence facilitate this movement [6, 3]. Many have theorised potential mechanisms that could induce contraction, such as filaments buckling, flexing or treadmilling [2, 5, 4]. However these explanations are complex and difficult to verify experimentally. We will instead implement the concept of "early motor drop-offs" presented In [1].

We will perform simulations utilising the agent based model developed in [1] to determine the effects of "early motor drop-offs" on the contractility of the stress fibre. We will then derive an appropriate homogenisation limit of the agent based model in the form of a fluid-type continuum model to support the findings of the simulations conducted.

Statement of Authorship

The agent based model seen in Section 2.2 was largely developed by Comino and Olez and was utilised in this study to run and document stress fibre simulations. Ryall, under the supervision and guidance of Olez, conducted the simulations using 'Julia' and developed the continuum fluid type model. Ryall wrote this report and also made the figures and graphs included utilising 'Julia' and 'R'.

1 1D model of a stress fibre

1.1 Model description

In our model (presented bellow) we have: *Actin filaments*, which make up the backbone of the stress fibre and consist of a barbed and pointed end. *Myosin motors*, that move along the actin thus determining the movement of the filaments. And *Focal adhesions*, which are the end points of the stress fibre and where the stress fibre grabs onto the cells external environment.

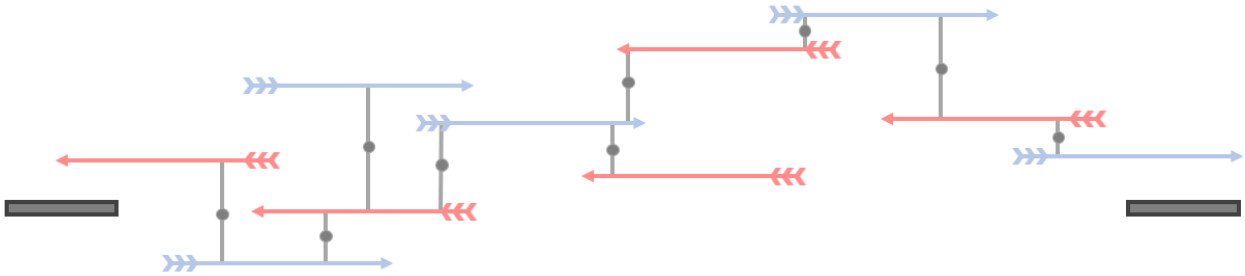

Figure 2: 1D representation of a stress fibre as described in the model

Figure 3: Interacting components present in our model

To facilitate movement there is an interaction between the filaments and motors with in the bundle. When two filaments and a motor overlap, the motor will attach itself to the two overlapping filaments. The motor will

move toward the barbed ends of the filaments crawling along the length until it reaches one of ends. When the motor reaches one of the barbed ends it will drop off. This motor can then reattach to any other filament pair that overlaps it.

To measure the contractile/expansive force experienced by the stress fibre we assume that the focal adhesions act like the tips of a stiff spring. The push/pull of actin filaments overlapping the focal adhesions dictates the movement of the adhesions. If the adhesions move closer together due to filament movement this will result in the distance between them decreasing which "compresses" the stress fibre spring. This results in the stress fibre experiencing a force of contraction. Conversely if the adhesions move further apart due to filament movement this will result in the distance between them increasing which "expands" the stress fibre spring. This results in the stress fibre experiencing a force of expansion.

1.2 Contractility analysis

When analysing filament and motor movement it can be seen that there are two distinct phases in their interaction. From when the motor attaches to the filaments to when the motor reaches the mid-point of the filaments, the filament pair is undergoing contraction (contraction phase). Conversely, in the period after the mid-point is reached to when the motor reaches the barbed end of the filaments (and then drops off) , the filament pair is undergoing expansion (expansion phase).

Figure 4: Two phases of motor-filament interaction

Since motor attachment can occur anywhere along the filament pair, all cases of attachment will result in the contraction phase always being shorter than or equal to the expansion phase. Thus overall, expansion will always be favoured in our stress fibres.

This contradicts what is seen in nature, where stress fibres are seen to contract to facilitate movement of cells. Therefore there must be a special interaction between the filaments and motors that is not yet accounted for in the model. To attempt to resolve this problem we propose the mechanism of "Early motor drop-offs".

1.3 Early motor drop-offs

We propose a solution to the contraction problem by implementing a new interaction into our model called "Early motor drop-offs": Instead of having our motors drop-off at the barbed end of the filaments we have them drop-off at a distance δ away from the barbed ends.

This aims to shorten the expansion phase as it will decrease the distance between the mid-point and the drop-off point therefore decreasing the period that filament pairs will be in the expansion phase.

Figure 5: Early motor drop-offs in motor-filament interaction

This concept stems from Tam's paper on flexible actin filaments [5] which showed that as myosin travels along the filaments, the filaments buckle causing the motor to drop off early before reaching the barbed ends.

Figure 6: Flexible actin filament buclking and early motor drop-off

2 Agent based model

2.1 Forces considered in our model

With these three interacting molecular components there are five main forces we consider in our agent based model.

- Drag force due to *cytoplasm viscosity*": Due to the viscus fluid that is present within the cell there is a drag force that opposes all filament moment.
- *Cross-linker* frictional force: Within stress fibres there are cross-linker proteins that form and connect between overlapping filaments, these proteins inhibit the movement thus generating a "friction" force between overlapping filaments.
- Myosin motor force: This is the force generated by the myosin motors as they travel along the filaments. this force is exerted on the filaments to pull the barbed ends closer to the motor.
- Focal adhesion friction: Filaments that overlap focal adhesions experience a "friction" force as the climb out of the extracellular matrix.

- Focal adhesion spring force: This force opposes the expansion and contraction of the stress fibre.

2.2 Force balance equations

Using these ideas we present the system of force balances developed in [1]. These force balance equations govern the model and its molecular components.

$$
\begin{aligned}
0 =& \xi \frac{\mathrm{d}x_i}{\mathrm{d}t} + \eta \sum_{j=1}^{N} O_{ij} \left(\frac{\mathrm{d}x_i}{\mathrm{d}t} - \frac{\mathrm{d}x_j}{\mathrm{d}t} \right) + \sum_{k=1}^{M} \Theta_{ik} \left(-F_s P_i + \frac{F_s}{V_m} \left(\frac{\mathrm{d}x_i}{\mathrm{d}t} - \frac{\mathrm{d}y_k}{\mathrm{d}t} \right) \right) \\
& + \zeta \sum_{j=A,B} O_{ij}^{a} \left(\frac{\mathrm{d}x_i}{\mathrm{d}t} - \frac{\mathrm{d}z_j}{\mathrm{d}t} \right), \text{ for } i = 1, \ldots, N \quad , \\
0 =& \sum_{i=1}^{N} \Theta_{ik} \left(F_s P_i - \frac{F_s}{V_m} \left(\frac{\mathrm{d}x_i}{\mathrm{d}t} - \frac{\mathrm{d}y_k}{\mathrm{d}t} \right) \right) \text{ for } k = 1, \ldots, M \quad , \\
0 =& k \left(z_B - z_A - L \right) - \zeta \sum_{i=1}^{N} O_{iB}^{a} \left(\frac{\mathrm{d}x_i}{\mathrm{d}t} - \frac{\mathrm{d}z_B}{\mathrm{d}t} \right) = 0 \quad , \\
0 =& k \left(z_B - z_A - L \right) + \zeta \sum_{i=1}^{N} O_{iA}^{a} \left(\frac{\mathrm{d}x_i}{\mathrm{d}t} - \frac{\mathrm{d}z_A}{\mathrm{d}t} \right) \quad . \qquad (1)
\end{aligned}
$$

The first equation is the equilibrium of forces acting on actin filament i of the N filaments in the system, with the terms representing: cytoplasm viscosity, Cross-linker friction and myosin motor force - in that order.

Similarly the second equation represents the force balance acting on myosin motor k of the M motors in the system, with the sole term representing the corresponding opposing force generated by the filaments opposing the myosin motor force.

The final two equations correspond to the force balances acting on each of the two focal adhesions with the terms representing: Focal adhesion spring force and Focal adhesion friction - in that order.

This system of force balance equations corresponds to an energy functional listed in A.3. We can then employ an energy minimisation scheme through the use of Julia to run the simulations presented bellow.

3 Simulations

3.1 Without early motor drop-offs

Utilising the agent model and the programming language Julia to implement the model we will first run simulations of the stress fibre without the implementation of early motor drop-offs. These simulations were run with the parameter set listed in A.1. When running these initial simulations it is found that on average expansion is always favoured over contraction. This aligns with the expansion bias outlined in Section 1.2.

3.2 With early motor drop-offs

We can now implement early motor drop-offs to observe the effects that this interaction has on the contractility of the stress fibre. After running these simulations it is found that by implementing these early motor drop-offs we have improved contractility which also aligns with Section 1.2.

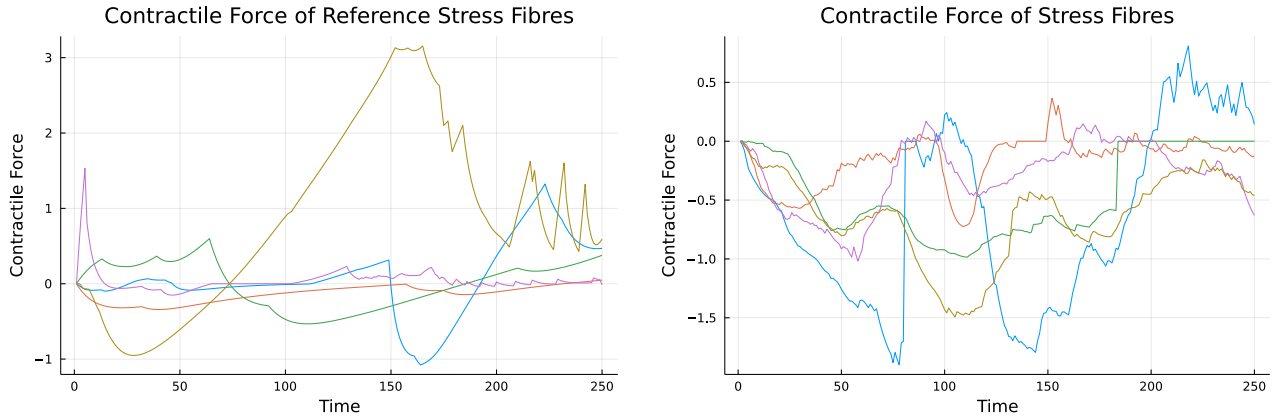

(a) 10 trials looking at contractile force over time without early motor drop-offs. Negative contractile force is contraction of the stress fibre conversely positive force is expansion

(b) 10 trials looking at contractile force over time with early motor drop-offs ($\delta = 1.0$). Negative contractile force is contraction of the stress fibre conversely positive force is expansion

Figure 7: contractile force Graphs generated by simulations

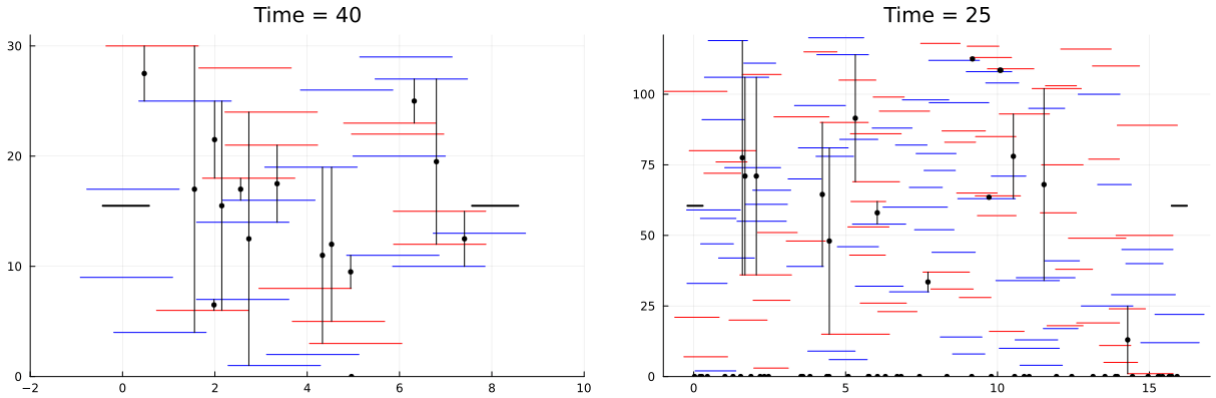

(a) Example frame of small simulation ($N = 30$)

(b) Example frame of large simulation ($N = 120$)

Figure 8: Example simulations run in Julia

3.3 Effect of early motor drop-offs

The question now is: what is the relationship between δ (the motor drop-off distance) and the contraction experienced by the fibre. We now run many simulations with different δ values to help determine this. In these simulations we also make the additional assumption that motors attach to filaments symmetrically i.e. motors

can only attach to filament pairs where both of the filaments barbed ends are the same distance from the motor.

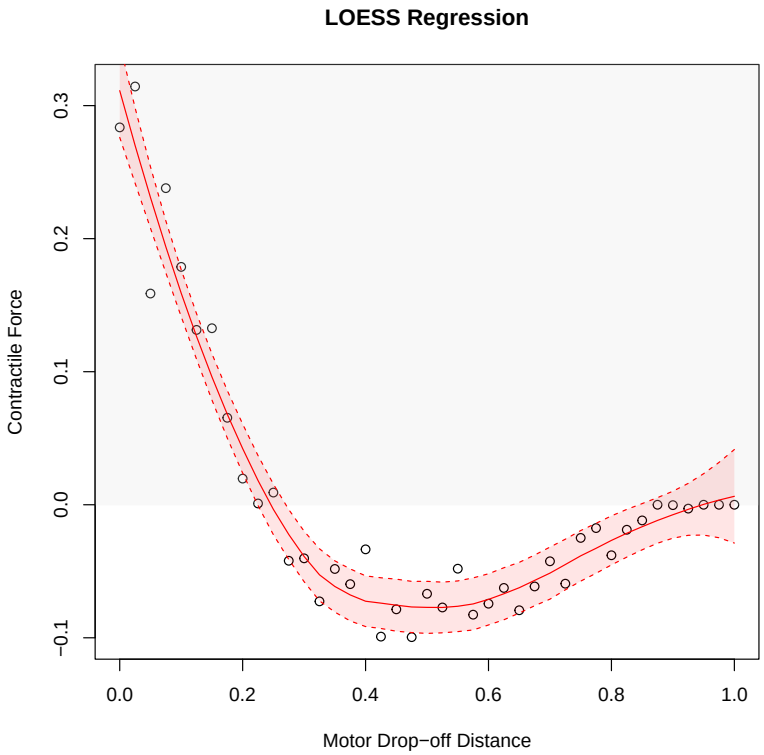

Figure 9: Relationship between δ and the average contractile force experienced by the fibre. Using actin filament length of $l = 1$ with 10 trials for each data point. Using a LOESS regression With 99% CI bands.

4 Continuum model

We now wish to support the simulated relationship between δ (motor drop-off distance) and contractility by developing a fluid-type continuum model for the stress fibre and deducing what this model can tell us about the relationship.

We work in the regime where actin filaments are short - and their abundance large.

In this model we assume that:

- Motors attach to filaments symmetrically i.e. motors can only attach to filament pairs where both of the filaments barbed ends are the same distance from the motor.
- Motors can only attach to filaments between the filaments pointed end "0" and its motor drop-off point "δ"

4.1 Description of quantities used

We introduce several quantities for this implementation of this model, the ones important to the paper are listed in this section.

We let, l denote the length of the actin filaments and L denote the length of the stress fibre. δ denotes the motor drop-off distance as defined above.

$\bar{\chi}(t, x, d)$ represents the density of motors at position x and at time t that are connected to anti parallel Actin filaments where both of filament's barbed ends are distance d away from x, $d \in [\delta, l]$. We do not need to consider motors connected to parallel filaments as these motors will just slide off towards the barbed ends of the filaments not producing any force.

5 First model for contractile force

To support these findings found by the simulations we can use the continuum model developed above. To do this we will determine the average position of myosin along the filaments. We look at average myosin position due to its strong link with contraction and expansion of the stress fibre.

5.1 Average motor position in relation to contractility

If the average motor position is between $0 \leq d \leq l/2$ relative to the filaments pair they are attached to then this indicates that filament pairs spend more time in the expansion phase than the contraction phase. And therefore the fibre should be expanding. Conversely if the average motor position is between $l/2 < d \leq l$ relative to the filaments pair they are attached to then this indicates that filament pairs spend more time in the contraction. And therefore the fibre should be expanding.

i.e. the closer the average motor position is to 0 the greater the force of contraction and loser the average motor position is to 0 the greater the force of expansion (i.e. decreased force of contraction), with $l/2$ being the point at which there is 0 force experienced in either direction. Therefore by subtracting a term of $l/2$ from the average motor position we will get an equation that is proportional to the contractile force experienced by the stress fibre.

5.2 Distribution of motor along filaments

Since motors can attach anywhere along the filament pair between $\delta \leq d \leq l$ and motors travel along the filaments toward the barbed end i.e. towards δ we can conlude the following relationship:

$$\bar{\chi}(t, x, d) = \begin{cases} (l - d)\bar{\chi}(t, x) & \delta \leq d \leq l \\ 0 & \text{else} \end{cases} \tag{2}$$

Where $\bar{\chi}(t,x)$ is the density of motors that are attached to the barbed ends of the filament pair and is a constant with respect to d. i.e. $\bar{\chi}(t,x) = \bar{\chi}(t,x,0)$

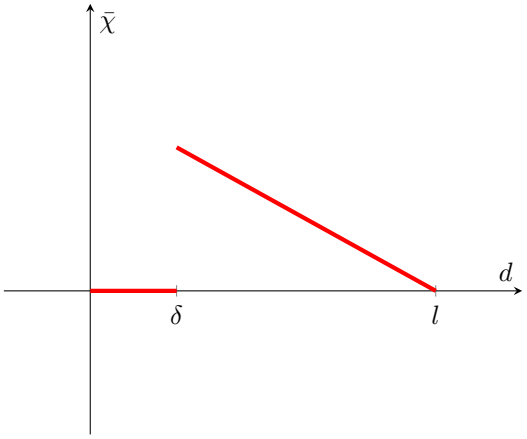

Figure 10: Density of myosin along filaments

5.3 Calculating average myosin position

The average myosin position relative to the actin filaments is given by the expected value of distance d along a filament weighted by density:

$$\int_{\delta}^{l} d\bar{\chi}(t,x,d)\mathrm{d}d$$

We can then normalise this value by having total density along a filament equal 1, which results in the average myosin position being given by:

$$\frac{\int_{\delta}^{l} d\bar{\chi}(t,x,d)\mathrm{d}d}{\int_{\delta}^{l} \bar{\chi}(t,x,d)\mathrm{d}d}$$

By utilising the result in equation (2) we find that:

$$\frac{\int_{\delta}^{l} d\bar{\chi}(t,x,d)\mathrm{d}d}{\int_{\delta}^{l} \bar{\chi}(t,x,d)\mathrm{d}d} = \frac{\int_{\delta}^{l} d(l-d)\bar{\chi}(t,x)\mathrm{d}d}{\int_{\delta}^{l}(l-d)\bar{\chi}(t,x)\mathrm{d}d} = \frac{\bar{\chi}(t,x)\int_{\delta}^{l} d(l-d)\mathrm{d}d}{\bar{\chi}(t,x)\int_{\delta}^{l}(l-d)\mathrm{d}d} = \frac{\left[\frac{ld^2}{2} - \frac{d^3}{3}\right]_{\delta}^{l}}{\left[ld - \frac{d^2}{2}\right]_{\delta}^{l}} = \frac{1}{3}(2\delta + l) \tag{3}$$

5.4 First model for contractility

The derived equation in combination with Section 5.1 tells us that: The stress fibre will experience contraction when average motor position i.e Equation (3) is $> l/2$ so therefore to adjust our model to be a measure of contractile force we subtract a term of $l/2$ from Equation (3). By switching the sign of this equation to ensure that contraction is a negative force (as in the simulations) our equation is now a model for contractility:

$$-\left(\frac{1}{3}(2\delta + l) - \frac{l}{2}\right) \quad \rightarrow \quad -\left(\frac{2}{3}\delta - \frac{l}{6}\right) \tag{4}$$

We now have that when Equation (4) < 0 the fibre is in contraction, conversely when when Equation (4) > 0 the fibre is in expansion. This equation is our first model for contractility based on δ. We now have our first model for contractile force.

We can see in this model that contraction will be experienced when (4) < 0 i.e. :

$$-\left(\frac{2}{3}\delta - \frac{l}{6}\right) < 0 \quad \rightarrow \quad \frac{2}{3}\delta - \frac{l}{6} > 0 \quad \rightarrow \quad \frac{2}{3}\delta > \frac{l}{6} \quad \rightarrow \quad 2\delta > \frac{l}{2} \quad \rightarrow \quad \delta > \frac{l}{4}$$

These equations therefore tell us that the fibre should on average experience contraction when $\delta > \frac{l}{4}$ and expansion when $\delta < \frac{l}{4}$.

We can now compare our first model i.e. Equation (4) with the simulated relationship between δ and fibre contractility.

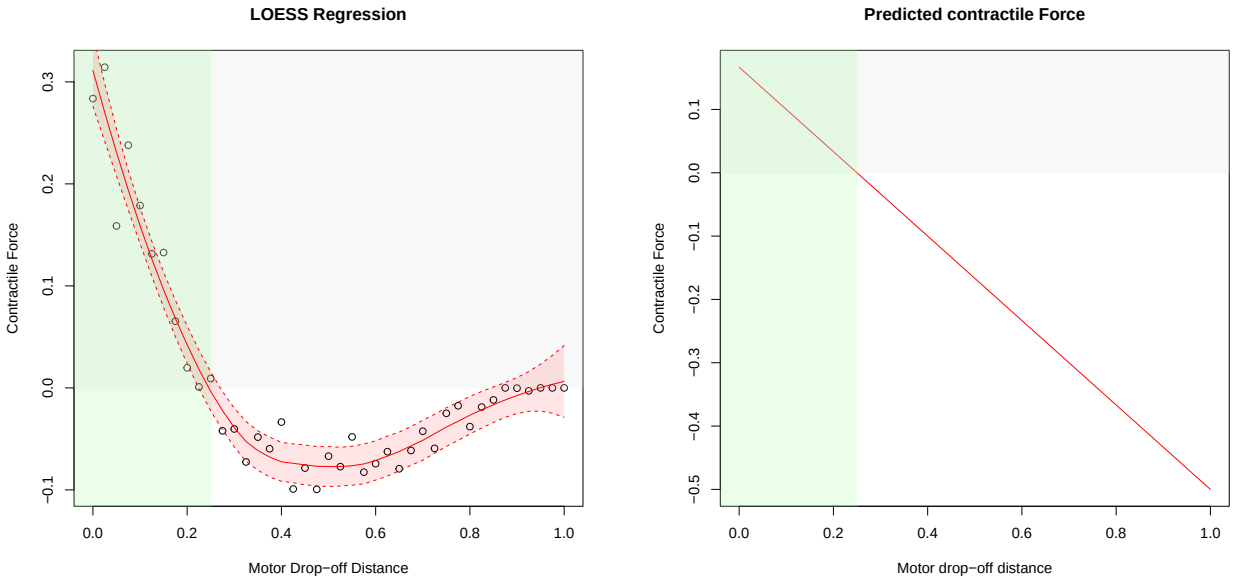

(a) Relationship between early motor drop-off distance δ and the average contractile force experienced by the fibre (using actin filament length of $l = 1$) as seen in simulation

(b) Relationship between early motor drop-off distance δ and the average contractile force as predicted by model one

Figure 11: Comparison of model one to the simulated data

We overlay the region the model predicts should undergo expansion with green and can see that this aligns with the simulated result. Thus supporting the relationship present in the simulations.

6 Second model for contractile force

The first model above is shown to predict and demonstrate the correct region of contraction however as δ becomes large its fit to the simulated relationship deviates. Hence we aim to improve our model by accounting for additional features, namely the proportion of active myosin.

6.1 Proportion of active myosin in relation to contractility

When considering our first model we did not account for the fact that as motor drop off distance δ increases the proportion of motors that are attached to filaments decreases.

This is due to the fact that motors can only attach to filaments in the range between the filaments pointed end at distance: "l" and the drop-off point at: "δ" and therefore as δ increases towards l the range that the motor can attach decreases.

The decrease in attached motors means that there are fewer active motors in the fibre. Fewer active motors leads to less force being exerted within the fibre and therefore a decreased contractile force. This means that the contra tile force is proportional to the proportion number of active motors in the fibre.

6.2 Proportion of active motors

In our model, motor attachment works as follows: for each free motor, two random filaments that overlap the motor are chosen for attempted attachment. If the motor can attach to the both filaments, it does, and the motor becomes active for that time step. However if the motor is unable to attach to both filaments or there are less than two filaments overlapping the motor the motor will not be active for that time step.

Before motor drop-offs were introduced the motor had a width l where it could attach. Now with the introduced drop-offs there is a shorter width where it can attach: $l - \delta$.

The probability of a motor that is overlapping a filament being within the range of attachment is equal to:

$$\left(\frac{l-\delta}{l}\right)$$

In our continuum model we consider the regime where filament abundance is large and therefore we can assume that motors will always have at least two overlapping filaments.

Hence the probability that a motor will be able to attach to both chosen filaments and therefore be active is given by:

$$\left(\frac{l-\delta}{l}\right)^2 \tag{5}$$

Therefore Equation (5) gives the proportion of active myosin.

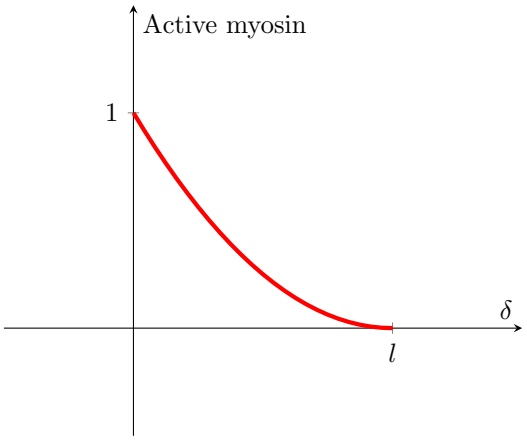

Figure 12: Proportion of active myosin

6.3 Second model for contractility

By accounting for this new interaction in our model we can develop a new equation for contractile force comprised of the product of Equation 4 and 5:

$$-\left(\frac{2}{3}\delta - \frac{l}{6}\right)\left(\frac{l-\delta}{l}\right)^2 \tag{6}$$

We can now compare our new model, Equation (6), with the simulated relationship between δ and contractility.

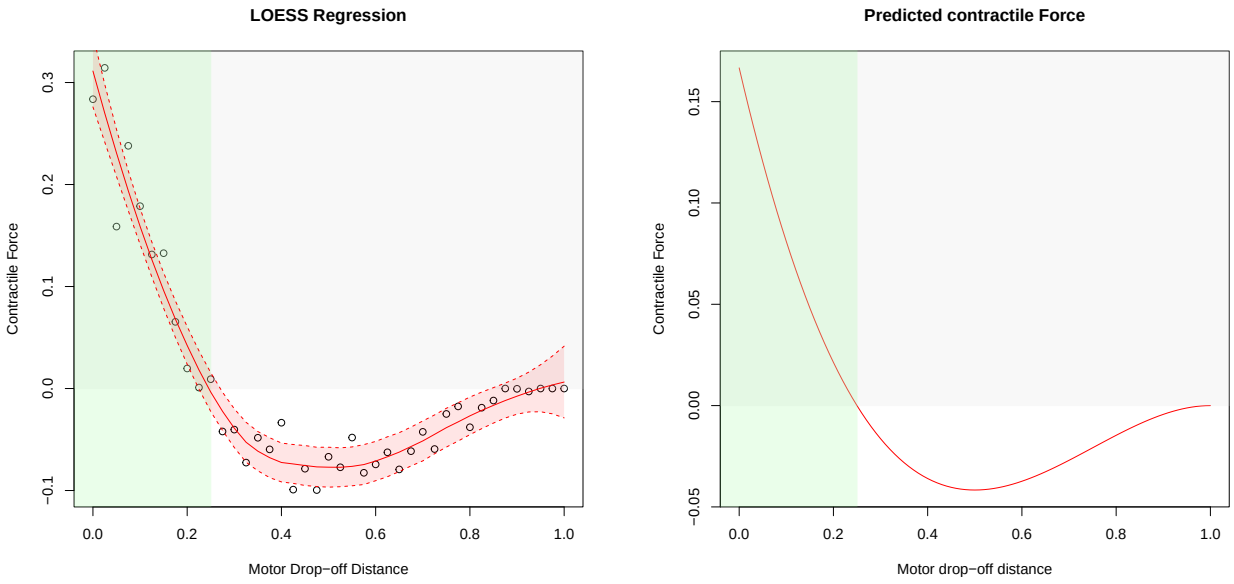

(a) Relationship between early motor drop-off distance δ and the average contractile force experienced by the fibre (using actin filament length of $l = 1$) as seen in simulation

(b) Relationship between early motor drop-off distance δ and the average contractile force as predicted by model 2

Figure 13: Comparison of model one to the simulated data

This new model predicts and aligns with the outcomes of the simulations much better than the original model especially for large δ. However, the the scaling is not accurate due to the fact that we have not accounted for dimensional constants.

7 Discussion and Conclusion

Within this report it was found that: The implementation of early motor drop-offs results in improved contractility of stress fibres when simulated using our agent based model. We also found that by converting to a continuum model and utilising average myosin position a closed form for effective contractility as given by delta can be found. Further more, it was observed that by accounting for the additional factor of myosin activity the model could be greatly improved especially for large δ.

One main point that warrants further investigation is the introduction of dimensional constants into the final model in order to resolve the issue of scaling. In an attempt to do this we converted our filament force balance equation into continuous quantities in an attempt to derive an appropriate limit for contractile force that includes dimensional constants. However at the conclusion of this research period this was not completed and should we investigated further. The conversion, scaling, non-dimensionalization and expansion can be found in Appendix A.2.

Acknowledgments

A big thanks is necessary to my supervisor Dietmar. Without him none of this would have been possible. His unwavering help and support has been vital for this project and his patience and perseverance was unrivaled when it came to teaching me the ropes.

References

[1] Emma Comino and Dietmar Oelz (2022). Actomyosin structures in stress fibres. Honours thesis produced in 2022.

[2] Lenz, M., Thoresen, T., Gardel, M. L., and Dinner, A. R. (2012). Contractile units in disordered actomyosin bundles arise from f-actin buckling. *Phys. Rev. X*, 108:238107.

[3] Murrell, M., Oakes, P., Lenz, M., and Gardel, M. (2015). Forcing cells into shape: the mechanics of actomyosin contractility. *Nat. Rev. Mol. Cell Biol.*, 16:486–498.

[4] Oelz, D. B., Rubinstein, B. Y., and Mogilner, A. (2015). A combination of actin treadmilling and cross-linking drives contraction of random actomyosin arrays. *Biophysical Journal*, 109(9):1818–1829.

[5] Tam, A. K. Y., Mogilner, A., and Oelz, D. B. (2022). F-actin bending facilitates net actomyosin contraction by inhibiting expansion with plus-end-located myosin motors. *bioRxiv*.

[6] Thoresen, T., Lenz, M., and Gardel, M. L. (2011). Reconstitution of contractile actomyosin bundles. *Biophysical Journal*, 100(11):2698–2705.

[7] Tojkander, S., Gateva, G., and Lappalainen, P. (2012). Actin stress fibers – assembly, dynamics and biological roles. *J Cell Sci*, 125(8):1855–1864.

A Appendix

A.1 Table of parameter values used

These tables summarise the parameter values used in the simulation of the stress fibres utilising the agent based model in Julia.

Description	Symbol	Value
Drag friction on actin filaments	ξ	0.0000001 pN s μm^{-2}
Drag friction on edge actin filaments	ρ	10 pN s μm^{-2}
Spring constant of stress fibre	k	10 pN μm^{-1}
Length of focal adhesions	$\bar{l}$	1 µm
Time step	Δt	0.1 s
Number of time steps	T	250

Table 1: List of reference parameters chosen.

Description	Symbol	Value
Equilibrium length of stress fibre	L	8 µm
Length of actin filaments	l	2 µm
Number of actin filaments	N	20
Number of myosin motors	M	10
Stall force for myosin motors	F_s	5 pN
Load-free myosin velocity	V_m	0.5 µm s^{-1}
Effective viscous drag due to cross-linkers	η	15 pN s μm^{-2}
Motor drop-off distance	δ	0 µm

Table 2: List of physical reference parameters.

A.2 Continuum model of filament forces

Agent based model filament forces

$$\xi v_{xi} + \eta \sum_{j=1}^{N} O_{ij}\left(\dot{x}_i - \dot{x}_j\right) + \sum_{k=1}^{M} \Theta_{ik}\left(-F_s P_i + \frac{F_s}{V_m}\left(\dot{x}_i - \dot{y}_k\right)\right)$$
$$+\zeta \sum_{j=A,B} O_{ij}^{a}\left(\dot{x}_i - \dot{z}_j\right) = 0 \quad \text{for } i = 1, \ldots, N$$
$$\sum_{i=1}^{N} \Theta_{ik}\left(F_s P_i - \frac{F_s}{V_m}\left(\dot{x}_i - \dot{y}_k\right)\right) = 0 \quad \text{for } k = 1, \ldots, M$$
$$k(z_B - z_A - L) - \zeta \sum_{i=1}^{N} O_{iB}^{a}\left(\dot{x}_i - \dot{z}_B\right) = 0$$
$$-k(z_B - z_A - L) - \zeta \sum_{i=1}^{N} O_{iA}^{a}\left(\dot{x}_i - \dot{z}_A\right) = 0$$

Converting to continuum model

Agent Based Model		Continuum Model
$\xi \dot{x}_i$	$\Longleftrightarrow$	$\xi \rho^{\pm}(t,x) v^{\pm}(t,x)$
$+\eta \sum_{j=1}^{N} O_{ij}\left(\dot{x}_i - \dot{x}_j\right)$	$\Longleftrightarrow$	$+\eta \sum_{n=-1,+1} \int_{\mathbb{R}} O(x-y)(v^{\pm}(t,x) - v^{n}(t,y))\rho^{\pm}(t,x)\rho^{n}(t,y)dy$
$-\sum_{k=1}^{M} \Theta_{ik} F_s \left(P_i - \frac{\dot{x}_i - \dot{y}_k}{V_m}\right)$	$\Longleftrightarrow$	$-\int_{\mathbb{R}} \Theta^{\pm}(t,x,y) F_s \left(\pm 1 - \frac{v^{\pm}(t,x) - v^{\mp}(t,y)}{2V_m}\right) dy$
$+\zeta \sum_{j=A,B} O_{ij}^{a}\left(\dot{x}_i - \dot{z}_j\right)$	$\Longleftrightarrow$	$+\zeta \sum_{j=A,B} O^{a}(x - z_j)(v^{\pm}(t,x) - V(t,z_j))\rho^{\pm}(t,x)$
$= 0 \quad \text{for } i = 1, \ldots, N$	$\Longleftrightarrow$	$= 0 \quad \forall x \in \mathbb{R}$

After non-dimensionalization and scaling

$$\tilde{\xi}\tilde{D}^{\pm} + \tilde{\eta}\tilde{C}^{\pm} - \tilde{M}^{\pm} + \tilde{\zeta}\tilde{A}^{\pm} = 0$$

Where:

$$\tilde{D}^{\pm} = \frac{1}{\tilde{l}} \tilde{\rho}^{\pm}(\tilde{t},\tilde{x}) \tilde{v}^{\pm}(\tilde{t},\tilde{x})$$
$$\tilde{C}^{\pm} = \sum_{n=-1,+1} \int_{\mathbb{R}} \tilde{O}(\Delta\tilde{x}_y)(\tilde{v}^{\pm}(\tilde{t},\tilde{x}) - \tilde{v}^{n}(\tilde{t},\tilde{x} + \tilde{l}\Delta\tilde{x}_y))\tilde{\rho}^{\pm}(\tilde{t},\tilde{x})\tilde{\rho}^{n}(\tilde{t},\tilde{x} + \tilde{l}\Delta\tilde{x}_y)\mathrm{d}\Delta\tilde{x}_y$$
$$\tilde{M}^{\pm} = \int_{\mathbb{R}} \tilde{\tilde{\chi}}\left(\tilde{t}, \tilde{x} - \tilde{l}\left(\frac{1}{2} - \tilde{d}\right), \frac{1}{2} \mp \left(\frac{1}{2} - \tilde{d}\right)\right)\left(\pm 1 - \frac{\tilde{v}^{\pm}\left(\tilde{t},\tilde{x}\right) - \tilde{v}^{\mp}\left(\tilde{t}, \tilde{x} - 2\tilde{l}(\frac{1}{2} - \tilde{d})\right)}{2}\right)\mathrm{d}\tilde{d}$$
$$\tilde{A}^{\pm} = \sum_{j=A,B} \tilde{O}^{a}(\Delta\tilde{x}_z)\left(\tilde{v}^{\pm}\left(\tilde{t},\tilde{x}\right) - \tilde{V}\left(\tilde{t}, \tilde{x} + \tilde{l}\Delta\tilde{x}_z\right)\right)\tilde{\rho}^{\pm}\left(\tilde{t},\tilde{x}\right)$$

After Symmetrization and Perturbation

$$0 = \xi(D^+ + D^-) + \eta(C^+ + C^-) + (M^+ + M^-) + \zeta(A^+ + A^-)$$

$$0 = \xi(D^+ - D^-) + \eta(C^+ - C^-) + (M^+ - M^-) + \zeta(A^+ - A^-)$$

Where:

$$\begin{aligned}
D^+ + D^- &= \frac{1}{l}(v_0\rho_0 - \bar{v}_0\bar{\rho}_0) + O(l^0) \\
D^+ - D^- &= \frac{1}{l}(v_0\bar{\rho}_0 - \bar{v}_0\rho_0) + O(l^0) \\
C^+ + C^- &= -\frac{l^2}{12}\partial_x\left(\rho_0^2\partial_x\left(v_0 + \frac{\bar{\rho}_0\bar{\bar{v}}_0}{\rho_0}\right)\right) + O(l^3) \\
C^+ - C^- &= \bar{v}_0(\rho_0^2 - \bar{\rho}_0^2) + O(l^1) \\
M^+ + M^- &= \frac{-2l}{3}(2\delta + l)\partial_x[\bar{\mu}_0(1 - \bar{v}_0)] + O(l^3) \\
M^+ - M^- &= -2\bar{\mu}_0(1 - \bar{v}_0) + O(l^1) \\
A^+ + A^- &= \sum_{j=A,B} \rho_0\left(v_0\rho_0 - \bar{v}_0\bar{\rho}_0 - V_0^j\rho_0\right) + O(l^1) \\
A^+ - A^- &= \sum_{j=A,B} \rho_0\left(v_0\bar{\rho}_0 - \bar{v}_0\rho_0 - V_0^j\bar{\rho}_0\right) + O(l^1)
\end{aligned}$$

A.3 Agent based model energy functional

The listed force balance equations were derived from the following energy functional:

$$\begin{aligned}
E[\mathbf{x},\mathbf{y},\mathbf{z}] = \xi\sum_{i=1}^{N}\frac{(x_i - x_i^n)^2}{2\Delta t} + \eta\sum_{i=1}^{N}\sum_{j=1}^{N}\frac{O_{ij}}{2}\frac{\left(x_i - x_j - (x_i^n - x_j^n)\right)^2}{2\Delta t} \\
+ \sum_{i=1}^{N}\sum_{k=1}^{M}\Theta_{ik}\left(-F_s(x_i - y_k)P_i + \frac{F_s}{V_m}\frac{\left(x_i - y_k - (x_i^n - y_k^n)\right)^2}{2\Delta t}\right) \\
+ \frac{k}{2}\left(z_B - z_A - L\right)^2 + \rho\sum_{i=1}^{N}\sum_{j=A,B}O_{ij}^a\frac{\left(x_i - z_j - (x_i^n - z_j^n)\right)^2}{2\Delta t}
\end{aligned}$$